Microporous and Mesoporous Materials 206 (2015) 127–135

Contents lists available at ScienceDirect

Microporous and Mesoporous Materials

journal homepage: www.elsevier.com/locate/micromeso

Controlled synthesis of tunable nanoporous carbons for gas storage and supercapacitor application

Kolleboyina Jayaramulu [a], Kasibhatta Kumara Ramanatha Datta [b], Konda Shiva [c], Aninda J. Bhattacharyya [c], Muthusamy Eswaramoorthy [b], Tapas Kumar Maji [a,*]

[a] Molecular Materials Laboratory, Chemistry and Physics of Materials Unit, Jawaharlal Nehru Centre for Advanced Scientific Research, Jakkur, Bangalore, India
[b] Nanomaterials and Catalysis Laboratory, Chemistry and Physics of Materials Unit, Jawaharlal Nehru Centre for Advanced Scientific Research, Jakkur, Bangalore, India
[c] Solid State and Structural Chemistry Unit, Indian Institute of Science, Bangalore, India

ARTICLE INFO

Article history:
Received 26 March 2014
Received in revised form 17 October 2014
Accepted 7 December 2014
Available online 13 December 2014

Keywords:
Nanoporous carbon
Metal–organic framework
Hydrogen storage
Carbon dioxide storage
Supercapacitor

ABSTRACT

A simple methodology has been developed for the synthesis of functional nanoporous carbon (NPC) materials using a metal–organic framework (IRMOF-3) that can act as a template for external carbon precursor (viz. sucrose) and also a self-sacrificing carbon source. The resultant graphitic NPC samples (abbreviated as NPC-0, NPC-150, NPC-300, NPC-500 and NPC-1000 based on sucrose loading) obtained through loading different amounts of sucrose exhibit tunable textural parameters. Among these, NPC-300 shows very high surface area (BET ≈ 3119 m^2/g, Langmuir ≈ 4031 m^2/g) with a large pore volume of 1.93 cm^3/g. High degree of porosity coupled with polar surface functional groups, make NPC-300 remarkable candidate for the uptake of H_2 (2.54 wt% at 1 bar, and 5.1 wt% at 50 bar, 77 K) and CO_2 (64 wt% at 1 bar, 195 K and 16.9 wt% at 30 bar, 298 K). As a working electrode in a supercapacitor cell, NPC-300 shows excellent reversible charge storage thus, demonstrating multifunctional usage of the carbon materials.

1. Introduction

Over the past decade, porous carbon materials have attracted a great deal of attention due to their potential applications in the fields of gas storage/separation, catalysis, fuel cell and biology [1–10]. Nanoporous carbons have received special attention compared to other contemporary porous materials because of its low density, chemical inertness and high thermal stability [11–13]. Among various techniques (both physical and chemical) to prepare nanoporous carbons, nanocasting approach using sacrificial template is an advantageous method owing to its fine control over pore size, surface area and pore volume [14–20]. In the past mesostructured silica, zeolites and clays have been utilized as hard templates for synthesizing hierarchical (meso/micro) porous carbons respectively [21–29]. Microporous carbon materials possessing high surface area are potential candidates for the adsorption and storage of small molecules such as hydrogen and carbon dioxide [30]. Recent reports suggests that materials are required to have appropriate balance between ultra microporosity, pore volume and surface area for high density hydrogen storage because of small kinetic diameter and low polarizability of hydrogen molecule [30]. Therefore, the synthesis of nanoporous carbon materials with high surface area and micropore (ultra-micropores) volume is of paramount importance, although it is not straightforward.

Metal–organic frameworks (MOFs) or porous coordination polymers (PCPs) are a novel class of crystalline materials and have various applications in gas storage, separation, catalysis, magnetism and drug delivery based on their structural topology, tunable pore size and environment [31–50]. MOFs with ordered functional porous environment combined with high crystallinity and thermal stability can also be utilized as templates for the preparation of high surface area porous carbons [51–56]. Using MOF as a template, Xu et al. first prepared porous carbons using furfuryl alcohol as an external carbon precursor [53]. Later, other research groups also reported porous carbons derived from MOF, with and without external carbon precursor [53]. Furthermore, porous carbon materials with tunable textural properties have received substantial attention, owing to their important industrial applications in catalysis, adsorption, chemical sensing and as a supercapacitor [27]. Therefore, the right choice of external carbon precursor and MOF is very critical to fabricate desired tunable nanoporous carbon sample. As MOFs offer ordered and tunable soft porous environment with various functional groups on organic linker, it is feasible to choose suitable carbon precursor which can be easily immobilized through an intermolecular host–guest interaction. Herein,

* Corresponding author. Tel.: +91 80 2208 2826; fax: +91 80 22082766.
E-mail address: tmaji@jncasr.ac.in (T.K. Maji).

http://dx.doi.org/10.1016/j.micromeso.2014.12.008
1387-1811/

we report a simple route for the synthesis of nanoporous carbon materials from IRMOF-3 {[$Zn_4O(NH_2\text{-}BDC)_3$]·xDMF}, (NH_2BDC = 2-amino-1,4-benzenedicarboxylate) which acts as a template for external carbon source (sucrose) and a self-sacrificing carbon precursor [60]. Although the synthesis of porous carbon from MOFs and external carbon precursor are well studied, their tunable textural property based on the loading of the external carbon precursor is yet to be accounted. This work reports synthesis, characterization, tunable surface area and pore volume (high ratio of micropore to mesopore) of various nanoporous carbon samples (NPCs) (NPC-0, NPC-150, NPC-300, NPC-500 and NPC-1000) obtained based on different loadings of sucrose in IRMOF-3. The beneficial influence of external carbon precursor to obtain high surface area NPC samples with high micro pore volume has been discussed in the context of gas storage and electrochemical supercapacitors. Among the NPC samples, NPC-300 shows high BET surface area of (3119 m^2/g) with a large pore volume (1.93 cm^3/g) which has been exploited for hydrogen and carbon dioxide storage and electrochemical double layer super capacitors.

2. Experimental section

2.1. Materials

All the reagents and solvents employed were commercially available and used as supplied without further purification. $Zn(NO_3)_2{\cdot}6H_2O$, 2-aminobenzenedicarboxylic acid, sucrose, were obtained from Aldrich Chemical Co.

2.2. Preparation of nanoporous carbon using IRMOF-3

IRMOF-3 was prepared according to the literature as reported by Yaghi et al. [57] using $Zn(NO_3)_2{\cdot}6H_2O$ (4.8 g, 16 mmol) and 2-aminoterephthalic acid (1.32 g, 8 mmol) in 30 mL of dimethylformamide (DMF) at 120 °C for 6 h. The resultant compound was filtered, thoroughly washed with DMF and then activated by guest exchange with ethanol (20 mL) for 7 days. The sample was then filtered and dried in vacuum at 130 °C. For the synthesis of porous carbon, we took desolvated IRMOF-3, different amounts of sucrose (X = 0, 150, 300, 500, 1000 mg), 8 μL of H_2SO_4 and then mixed together in 2 mL of water to form light yellow colored paste. This mixture was then kept in an oven for successive temperatures 100 °C for 6 h and 160 °C for 6 h. The resulting composites were then pyrolyzed in a nitrogen flow at 900 °C and kept under these conditions for 6 h to carbonize the composite. The NPCs were obtained after removal of ZnO species using 20% hydrochloric acid by filtration, washed several times with water–ethanol mixture followed by drying at 100 °C. The resultant carbons obtained by variation in sucrose content are denoted by "NPC-X", where X indicates that amount of sucrose used. The obtained samples were designated as NPCs (NPC-0, NPC-150, NPC-300, NPC-500 and NPC-1000) based on the different amount of sucrose loading. All the resultant NPCs were characterized by FT-IR, elemental analysis, thermogravimetric analysis, powder X-ray diffraction (PXRD), Energy dispersive X-ray analysis (EDS) and different microscopic techniques.

3. Characterization techniques

3.1. Physical measurements

The resultant NPC samples were characterized through different techniques. Powder X-ray diffraction (PXRD) patterns were recorded on a Bruker D8 Discover instrument using Cu-Kα radiation. The morphology and porous nature of NPCs examined with field emission scanning electron microscope (FESEM, FEI Nova-Nano SEM-600, Netherlands) and transmission electron microscope (TEM) (JEOL JEM-3010 with an accelerating voltage at 300 kV). The Raman spectra were recorded in backscattering arrangement, using 532 nm laser excitation using 6 mW laser power. Elemental analyses were carried out using a Thermo Scientific Flash 2000 CHN analyzer. FT-IR spectra were recorded using KBr pellets in the range 4000–400 cm^{-1} on a Bruker IFS-66v spectrophotometer. Thermogravimetric analysis (TGA) were carried out under nitrogen (flow rate of 50 mL/min) with Metler Toledo TGA-850 TG analyzer in the temperature range between 25 and 600 °C at a heating rate 3 °C/min.

3.2. Adsorption measurements

Adsorption studies of N_2 (77 K), CO_2 (195 K for NPC-300) and H_2 (77 K for NPC-300) for NPC samples prepared at 423 K under high vacuum, were carried out using QUANTACHROME AUTOSORB-1C analyzer. The adsorption isotherm of different solvents (like H_2O and C_6H_6, at 298 K) for NPC 300 was measured in the vapor state by using BELSORP-aqua-3 volumetric adsorption instrument from BEL, Japan. In the sample chamber (~12 mL) maintained at T ± 0.03 K was placed the adsorbent sample (100–150 mg), which had been prepared at 423 K in 10^{-1} Pa for 18 h prior to measurement of the isotherms. The adsorbate was charged into the sample tube, and then the change of the pressure was monitored and the degree of adsorption was determined by the decrease of the pressure in the equilibrium state. All operations were computer-controlled and automatic. High-pressure H_2 (77 K) and CO_2 (298 K) sorption measurements for NPC-300 was carried out on a fully computer controlled volumetric BELSORP-HP, BEL JAPAN high pressure instrument. All the gases used for high pressure measurements are scientific/research grade with 99.999% purity. For the measurements, approximately 300 mg sample was taken in a stainless-steel sample holder and degassed at 493 K for a period of 18 h under 0.1 Pa vacuum. The dead volume of the sample cell was measured with helium gas of 99.999% purity. Non-ideal correction for H_2 and CO_2 gases were made by applying virial coefficients at the respective measurement temperature.

3.3. Supercapacitor cell measurements

Investigations were carried out using NPC-300 as a working electrode in a cell containing 1.0 M aqueous H_2SO_4 solution as electrolyte, platinum wire as counter electrode and a saturated calomel electrode (SCE) as a reference electrode. All electrochemical characterizations were performed at room temperature. The composite working electrode was prepared by dispersing a mixture of NPC-300, polyvinyldifluoride (PVdF) binder and acetylene black in N-methyl-pyrrolidone (NMP) solvent. The three components were in the ratio 85:05:10 (w/w) in NMP and processed to form homogeneous slurry. The homogeneous mixture is pasted onto stainless steel (SS) current collector (0.5 × 0.5 cm^2) and electrodes were dried at 120 °C for 12 h under vacuum.

4. Results and discussion

4.1. Synthesis and characterization NPCs

The step-wise synthesis of various nanoporous carbons obtained from sucrose and IRMOF-3 is illustrated in Fig. 1. IRMOF-3 {$Zn_4O(NH_2\text{-}BDC)_3$} has a three dimensional structure consist of an oxo-centred {$Zn_4O(CO_2)_6$} secondary building units connected by NH_2-BDC linkers. Framework has 3D channels (dimensions of 18 × 18 $Å^2$) decorated with basic –NH_2 functional

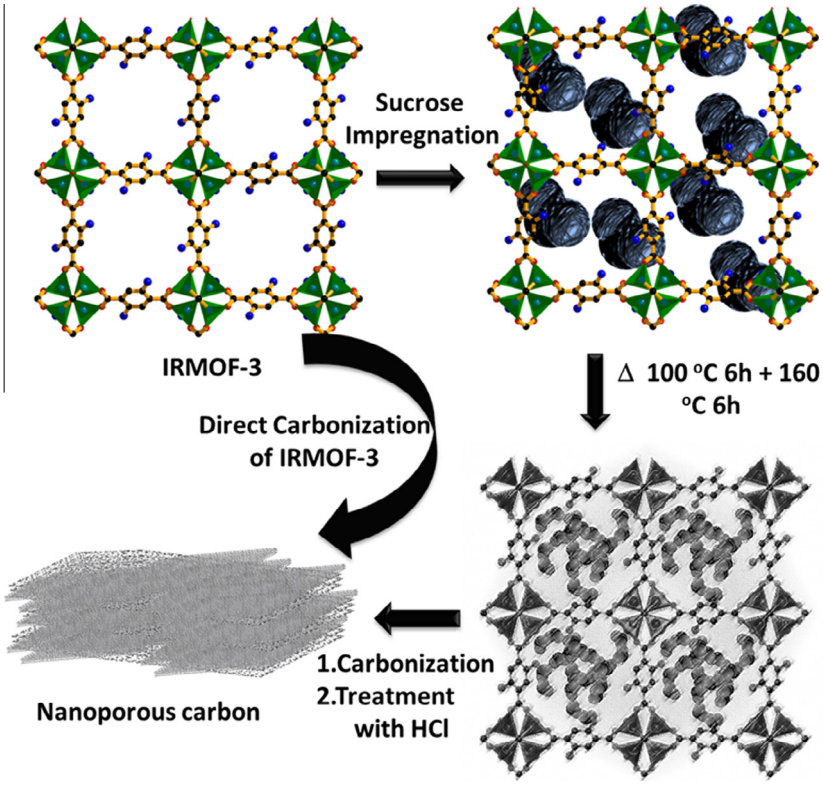

Fig. 1. Flowchart showing detailed synthetic methodology of IRMOF-3 derived nanoporous carbon.

groups and possessing a surface area of 2371 m^2/g. We surmise that, the inclusion of sucrose inside the pores (amine functionalized pore surface) is facilitated by its hydrogen bonding interaction. Sucrose loaded IRMOF-3 has retained structural integrity as revealed by powder XRD pattern (Fig. S1). Sucrose infiltrated IRMOF-3 was heated at 100 and 160 °C for the polymerization of sucrose and then resulting composite is carbonized under a nitrogen atmosphere at 900 °C resulting in a black colored powder.

The EDS analysis and PXRD pattern of these carbonized samples suggest the presence ZnO nanoparticles (Fig. S2). The wide angle PXRD pattern of the carbonized sample exhibit peaks corresponding to hexagonal phase of wurtzite (Fig. S2 (left)). After treating the carbonized samples with HCl solution (20%) followed by through washing with a water/ethanol mixture yields pure nanoporous carbon samples. The same procedure was adopted with various sucrose loadings to prepare different NPCs (see Section 2). The purity of all resultant NPC samples after HCl treatment is confirmed through elemental (CHN) analysis (Table S1). FT-IR spectra of all NPCs show —C=C— vibrational bands along with oxygen containing carboxyl (—COOH) and hydroxyl (—OH) functional groups (Fig. S3 for NPC-300). The PXRD patterns of all the resultant NPC samples are shown in Fig. S4 (NPC-0, NPC-150, NPC-500 and NPC-1000) and Fig. 2 (left) (for NPC-300). Interestingly, all NPC samples after treating with HCl exhibited two major broad peaks centered at $2\theta = 24.5°$ and 44.3° corresponding to (002) and (101) planes respectively, which resembles the structural signature of nanoporous carbons. Further Raman spectroscopy measurements were performed to study the local structure of the NPC samples. Raman spectra of NPC samples are provided in Figs. 2 (right) and S5, showing two major broad peaks centered at ~1350 and ~1629 cm^{-1} and are attributed to D- and G-bands respectively. The relative ratios of the G band to D band are almost constant ($I_G/I_D \sim 1.2$) in all the NPC samples. The ratio of the intensities of D to G bands signify the degree of crystallization of the graphitic carbon and suggests in all NPC samples the local carbon structure has both graphitic and disordered carbon atoms [28].

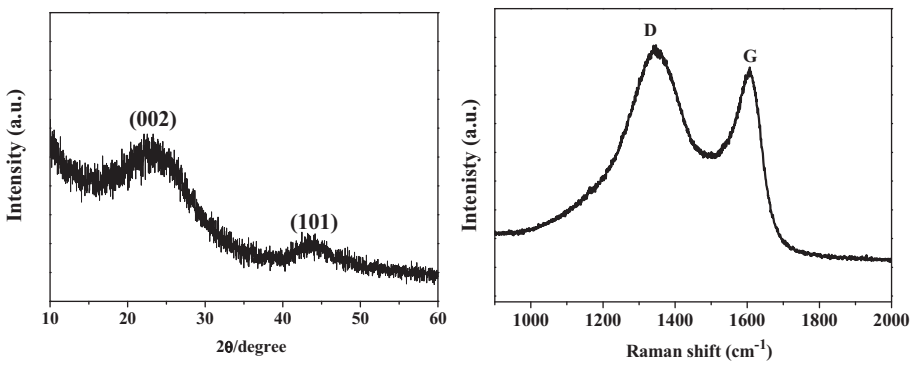

Fig. 2. (left) Powder X-ray pattern; (right) Raman spectra of NPC-300.

Furthermore field-emission scanning electron microscopy (FESEM) analyses were performed to understand the morphology of the resulting porous carbons and also the effect of MOF on the resulting morphologies and overall surface textural characteristics (Figs. 3 and S6). FESEM images suggests that the original cubic morphology of the IRMOF-3 was not retained in the NPC samples, rather a different morphologies were observed in the various NPC samples. In case of NPC-300 well separated micron size rod or block shaped carbon particles was observed, whereas NPC-1000 revealed the aggregated sheets of carbon in micron size range. Other samples like NPC-0, NPC-150 and NPC-500 exhibit sponge like morphologies. However high-magnification images uncovered a wide range of pore sizes from micrometer to nanometer compared to defect free surfaces in IRMOF-3. High resolution transmission electron microscope (HRTEM) images reveal oriented multilayer domains in all the carbon samples and few indistinguishable parallelly stacked graphene sheets (Fig. 4). Similar structure was observed in previously reported MOF derived carbon materials [53]. In agreement with PXRD and Raman spectra, all the samples contain high degree of disordered graphitic layers. The bicontinuous three-dimensional network of nanosized carbon particles with small grain sizes (about 5–10 nm) resulted the hierarchical porosity. These results suggest that surface texture and characteristics could be tuned to some extent by changing the content of the carbonizing agents.

4.2. Textural parameters for NPC samples

Nitrogen adsorption experiments (at 77 K) were performed to examine the surface textural characteristics of the NPC samples

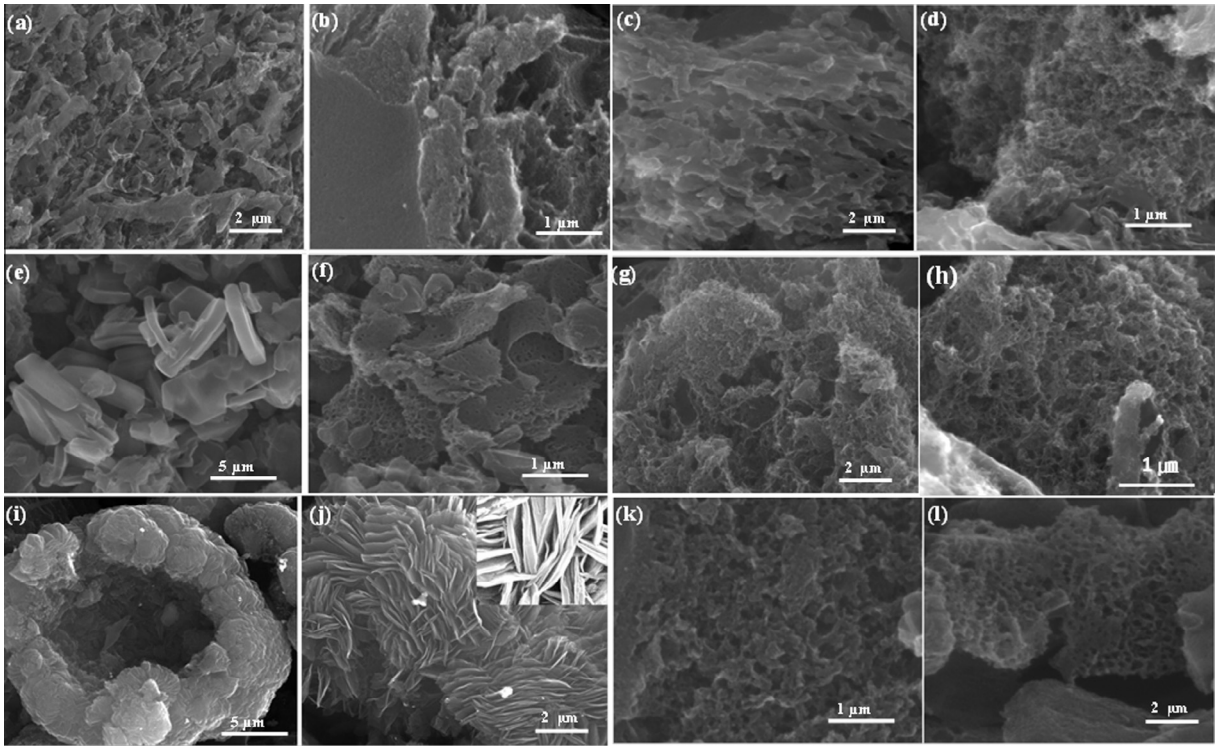

Fig. 3. FESEM images of all NPC samples; (a and b) NPC-0, (c and d) NPC-150, (e and f) NPC-300, (g and h) NPC-500, (i and j) NPC-1000, (k and l) sucrose derived carbon.

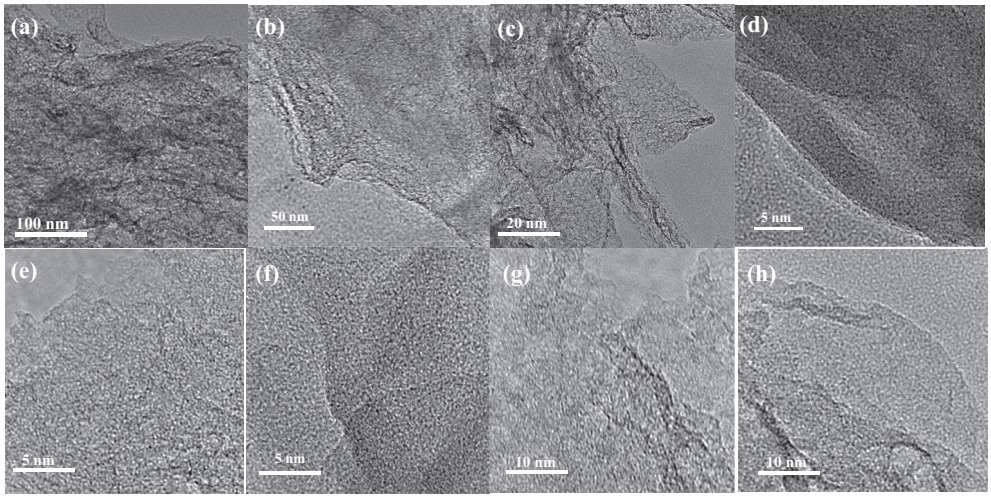

Fig. 4. TEM images of all NPC samples; (a) NPC-0, (b) NPC-150, (c and d) NPC-300, (e) NPC-500, (f and g) NPC-1000, (h) sucrose derived carbon.

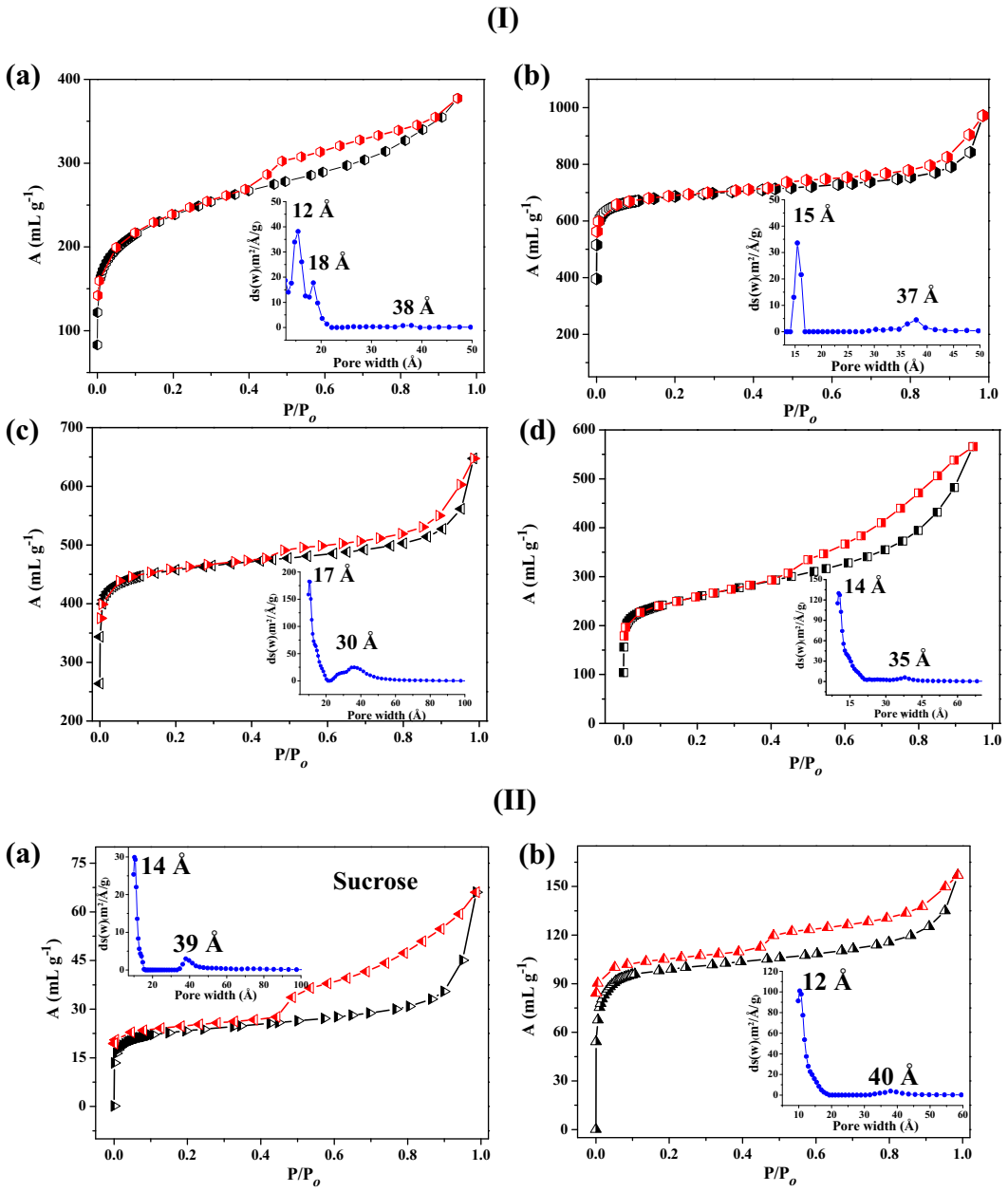

Fig. 5. (I) Nitrogen adsorption isotherms of (a) NPC-150, (b) NPC-300, (c) NPC-500 and (d) NPC-1000 (inset showing pore size distribution respective samples obtained from NLDFT method). (II) Nitrogen adsorption isotherms of carbons derived from sucrose, and IRMOF-3 (NPC-0) samples (inset showing pore size distribution respective samples obtained from NLDFT method).

Table 1
Textural parameters of the resultant NPC samples.

Sample	S_{BET} (m^2/g)[a]	S_{Lang} (m^2/g)[b]	S_{micro} (m^2/g)[c]	S_{meso} (m^2/g)[d]	S_{meso}/S_{micro}	V_t (cm^3/g)[e]	V_{micro} (cm^3/g)[f]	V_{meso} (cm^3/g)[g]	$V_{meso/micro}$ (cm^3/g)
Sucrose	258	391	117	141	1.2	0.17	0.08	0.09	1.125
NPC-0	392	581	299	93	0.31	0.409	0.36	0.049	0.136
NPC-150	1022	1567	898	124	0.13	0.65	0.58	0.07	0.121
NPC-300	3120	4031	2987	133	0.03	1.93	1.89	0.04	0.024
NPC-500	1761	2687	1692	69	0.04	0.74	0.58	0.16	0.103
NPC-1000	1077	1622	994	83	0.08	0.435	0.245	0.19	0.175

[a] S_{BET} is the BET specific surface area.
[b] S_{Lang} is the Langmuir specific surface area.
[c] S_{micro} is the *t*-plot specific micropore surface area calculated from the N_2 adsorption–desorption isotherm.
[d] S_{meso} is the specific mesopore surface area estimated by subtracting S_{micro} from S_{BET}.
[e] V_t is the total specific pore volume determined by using the adsorption branch of the N_2 isotherm at $P/P_0 = 0.99$.
[f] V_{micro} is the specific micropore volume calculated by NLDFT.
[g] V_{meso} is the specific micropore volume calculated by subtracting V_{micro} from V_t.

[Fig. 5](I) for NPC-150, NPC-300, NPC-500, NPC-1000 and Fig. 5(II) for NPC-0 and Sucrose derived carbon] (Table 1). All IRMOF-3 derived samples exhibit combined characteristics of type I and type IV isotherms with a steep uptake at low pressure regions, suggesting the dominant microporous nature in the carbon samples. The hysteresis in desorption curve in $P/P_0 > 0.4$ for all the samples can be accounted for the existence of mesopores as well. The BET surface area for NPC-150, NPC-300, NPC-500 and NPC-1000 were found to be 1022, 3119, 1760 and 1077 m^2/g respectively. The corresponding Langmuir surface areas are given in Table 1. The BET surface areas for the NPC samples derived exclusively from sucrose and IRMOF-3 were 258 and 391 m^2/g, respectively. Among the various NPC samples, NPC-300 shows the highest BET surface area and Langmuir surface area is about 4031 m^2/g with a micro pore volume of 1.93 cm^3/g.

All the samples show wide pore size distribution as obtained from Non-Local Density Functional Theory (NLDFT) method. The micropore sizes are in the range of 1.2–1.8 nm whilst the mesopore sizes fall in the range of 3–4 nm. Furthermore, the surface areas related to micropore were calculated from the *t*-plot that suggested that NPC-300 has a very high micropore surface area (2984 m^2/g) and then decreases with increasing sucrose content, in case of NPC-1000 the corresponding value is 994 m^2/g. On the other hand mesopore surface area increases with increasing sucrose content after NPC-300. The total pore volumes were determined through adsorption profiles up to $P/P_0 = 0.99$, whereas micro pore volumes were obtained from (NLDFT) method and details are compiled in Table 1. We have clearly shown that hierarchically (micro and meso) nanoporous carbons (NPCs) with tunable porosity can be prepared based on loading of different amount of external carbonizing agent. The BET surface area (S_{BET}) measured from N_2 adsorption slowly increases from NPC-0 to NPC-300 and then decreases gradually. In addition the mesopore to micropore surface area (S_{meso}/S_{micro}) and mesopore to micropore volume (V_{meso}/V_{micro}) can also be varied by the different amount of sucrose loading. This is the first systematic study where textural properties can be systematically tuned in a MOF derived carbon materials by using an external carbon precursor. The BET surface area of NPC-300 is second highest reported in MOF derived carbon materials using external carbon source and is comparable to porous carbon derived from ZIF-8 without additional carbon precursor [53]. Upon encapsulation and subsequent polymerization of sucrose resulting in a small pores and concomitant decomposition of IRMOF-3, that acting as a template and self-sacrificing carbon precursor further contributed towards this high surface area. The high micropore surface area and pore volume in NPC-300 can be attributed to the optimum condition where maximum loading of the sucrose is possible in the pores of IRMOF-3 which resulting in micro pore after carbonization. It should be noted that the direct carbonization of sucrose and IRMOF-3 (NPC-0) exhibits major contribution of mesopores with less surface area as clearly observed in Fig. 5(II). The decrease in microporosity and increase in mesoporosity in NPC-500 to NPC-1000 probably due to the involvement of the surface adsorbed sucrose.

4.3. H_2 and CO_2 storage properties

Encouraged by the high surface area and micropore volume, we measured H_2 and CO_2 storage capacity for NPC-300 at different conditions. As shown in Fig. 6a (inset), H_2 uptake capacity is found

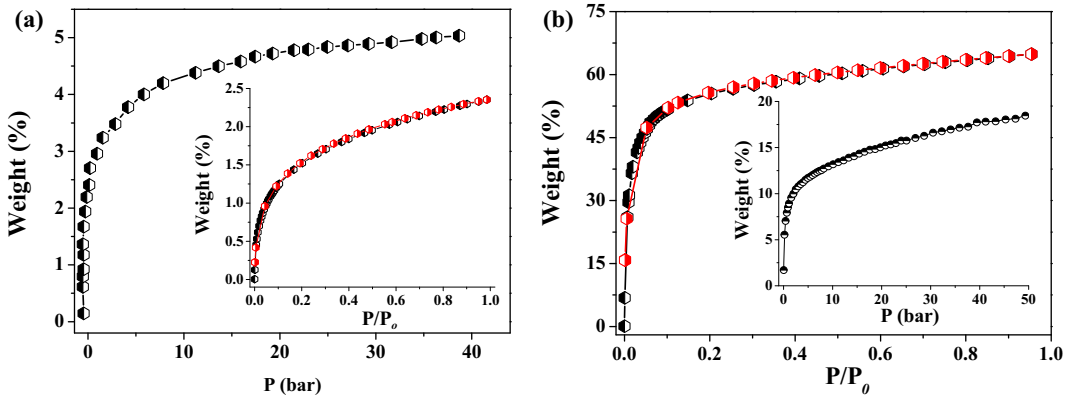

Fig. 6. (a) High pressure hydrogen adsorption isotherm for NPC-300, up to 40 bar at 77 K, (inset showing up to 1 atm 77 K), (b) CO_2 adsorption isotherm for NPC-300 1 atm at 195 K 1 atm (inset CO_2 uptake 30 bar at 298 K).

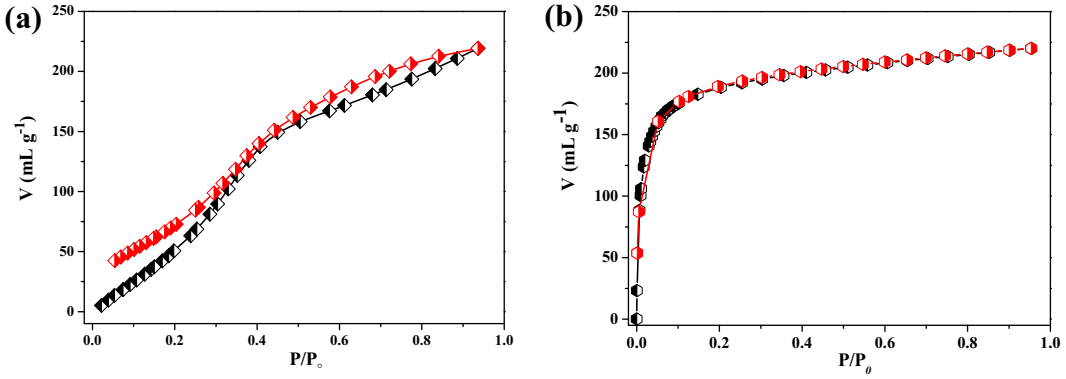

Fig. 7. Vapor sorption isotherm of NPC-300 for (a) H_2O, (b) C_6H_6 at 298 K (P_0 is the saturated vapor pressure of the adsorbates at the respective temperatures).

to be 2.45 wt% at 1 atm, at 77 K, much higher than the IRMOF-3 (1.3 wt% at 77 K, 1 atm). Sorption profile suggests complete reversibility without any hysteresis, indicating H_2 molecule are physisorbed. The storage capacity in this condition is comparable to the highest value reported so far for MOF derived carbon materials (see Table S2) and MOFs of similar surface area. This value is much higher than the activated carbons and zeolites [28]. The H_2 uptake capacity significantly increases at high pressure and it shows about 5.1 wt% at 40 bar, 77 K (Fig. 6a). This value is comparable to the best performances MOFs, including IRMOF-77, 176, HKUST, PCN-7 [54]. NPC-300 has high degree of microporosity which is probably beneficial for hydrogen uptake. To the best of our knowledge this is the highest storage capacity of hydrogen in NPC derived from a MOF template. This is attributed to the saturation at large number of adsorption sites at high pressure compared to the lower pressure. Further this material has been tested for CO_2 capture at various conditions and showed exceptionally high capacity of CO_2 uptake. At 195 K and 1 atm, the NPC-300 sample exhibited 64 wt% uptake capacity (Fig. 6b). Then we have tested at 298 K under high pressure and the uptake amount is 86 mL/g (16.9 wt%) at 30 bar (Fig. 6b (inset). The steep uptake at low pressure regions can be attributed to the strong interactions of CO_2 and micropore surface composed with the graphitic carbons as the former having large quadrupole moment which can effectively interact with π cloud of the NPC-300 sample. To understand the polarity of the pore surface in NPC-300 water and benzene vapor sorption were carried out at 298 K (Fig. 7). Benzene adsorption profile reveals a typical type I profile with steep uptake at low pressure regions whereas water vapor shows unusual type V isotherm with gradual uptake at low pressure regions (Fig. 7a). The onset steep uptake pressure is about $P/P_0 \sim 0.3$ and final uptake amount is about 220 mL/g at $P/P_0 \sim 1$ with small hysteresis at high pressure region. The final uptake amount by NPC-300 for benzene is 196 m^2g^{-1} (Fig. 7b). This variation in the adsorption behavior for benzene and water suggests the graphitic structure of NPC-300 interact well with nonpolar molecule like benzene [28]. This suggests strong hydrophobic character of the pore surfaces which is also supported by the water adsorption profile.

4.4. Supercapacitor application

Recently, multi-functional porous carbon materials with hierarchical porous structures have attracted considerable attention in electrochemical energy storage and conversion devices [15]. Supercapacitors are energy storage devices which display very fast charge–discharge rates over several thousands of cycles [58–63]. Their utility is being realized in various applications including electric vehicles. Based on the beneficial structural features, exploratory electrochemical investigations targeted at employing NPC-300 as a probable supercapacitor electrode. Electrochemical performance of NPC-300 based electrode was tested using cyclic voltammetry (CV) and galvanostatic (i.e. at constant current) discharge/charge cycles. Cyclic voltammograms (CVs) of porous carbon supercapacitors obtained in the potential range (−0.5 to 0.5) V at different sweep rates (10–100 mV/s) are shown in Fig. 8a. The above scan rate range was selected to investigate the profiles of the CV of NPC-300 and their proximity to the rectangular traces typically obtained for carbonaceous materials for supercapacitors.

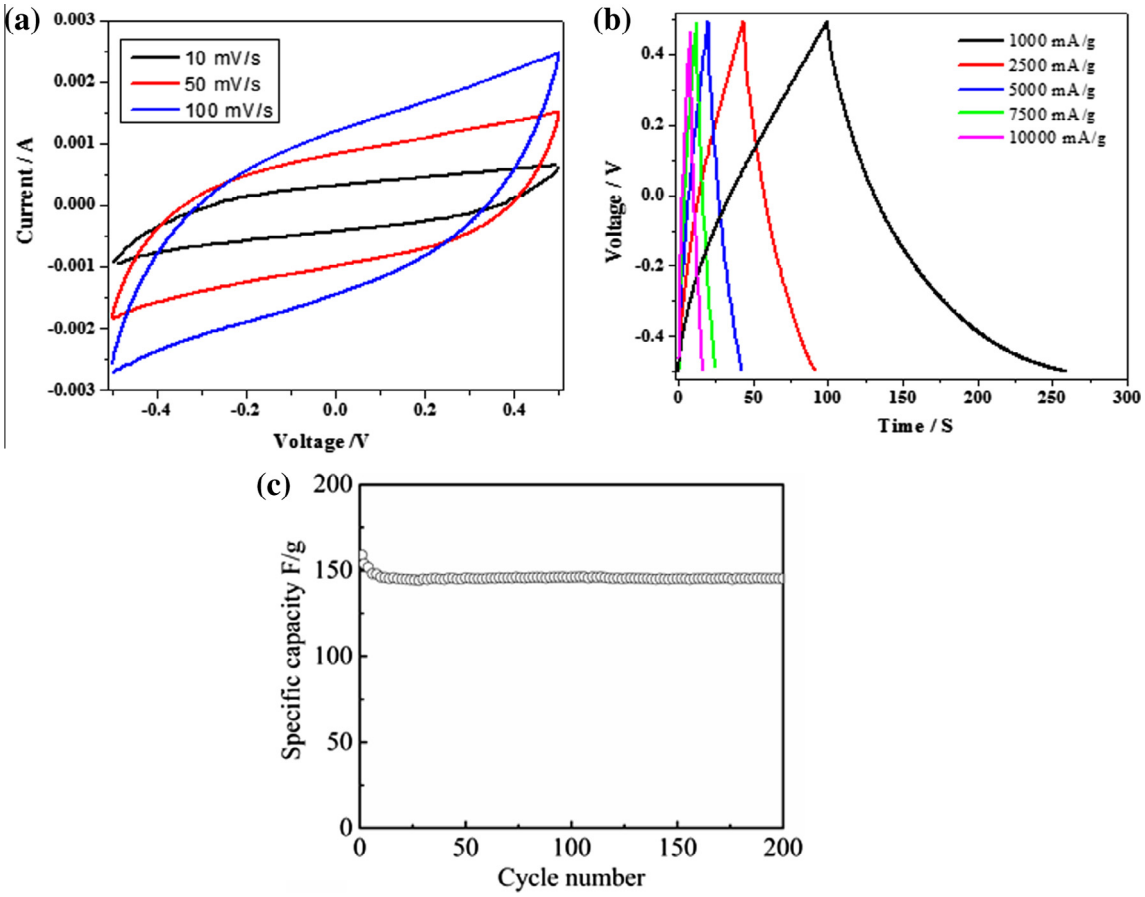

Fig. 8. Electrochemical characteristics of resultant NPC-300: (a) CV profiles investigated at different scan rates from 10 to 100 mV s^{-1} between −0.5 and 0.5 V in 1.0 M H_2SO_4 electrolyte using a three electrode capacitor, (b) galvanostatic charge–discharge curve at different current densities, and (c) galvanostatic charge/discharge cycling of nanoporous carbon measured at 1 A/g.

The measured CV curves have quasi-rectangular shape (≈10 mV/s) without any redox peaks indicating that the NPC-300 material showing a typical electric double-layer capacitive behavior. However, the deformation in the CV curves at high scan rate (≈100 mV/s) may be attributed to the various charge transport kinetics such as limited diffusion and migration of electrolyte ions into the bulk. As reported, these are depend on several factors such as pore size, morphology, chemical nature of the pores and degree of electrolyte filling [64]. As a result the charge transport (kinetics) in porous structure is complex and non-universal. More rectangular-like CV traces at higher scan rates may be achieved with additional optimizations with regard to materials synthesis, electrode composition and cell configuration. These are materials engineering issues very specific to supercapacitor performance optimization which is outside the scope of the present studies. Fig. 8b shows the galvanostatic charge/discharge measurements for NPC-300 electrode material supercapacitor at very high current densities of 1–10 A/g. The specific capacitances (calculated using $C = (I \times \Delta t)/(\Delta V \times m)$, where I is the discharge current, Δt is the discharge time from 0.5 to −0.5 V, ΔV is the voltage difference within the discharge time Δt, and m is the mass of porous carbon) calculated from the discharge curves are 159, 118, 111, 90 and 78 F/g at 1, 2.5, 5, 7.5 and 10 A/g, respectively. From the high capacity values and exceptional stability (Fig. 8c) it is concluded that the NPC-300 has considerable potential as an electrode in supercapacitors. The decrease in specific capacitance of NPC-300 electrode is with increasing current densities is due to the increase of iR (voltage) drop and slow ion transfer at high current density. The graphitic environment, hierarchical porosity, high surface area made NPC-300 as a good supercapacitor materials which is comparable to other porous carbons derived from various MOFs. Electrochemical impedance spectroscopy was measured to further understand the charge transport kinetics in the porous NPC-300. The Nyquist plot in the range (1-10^6) Hz for the NPC-300 is shown in Fig. S7. The nearly vertical spike suggests good capacitor behavior of the cell. The equivalent series resistance obtained from the intercept of the spike with the real Z' axis (the x-axis) is approximately 4 Ω. The low values strongly suggest that NPC-300 have a very low resistance with good ionic response. The graphitic environment, hierarchical porosity, high surface area make NPC-300 a good supercapacitor materials which is comparable to other porous carbons derived from various MOFs (Table S3).

5. Conclusions

In conclusion, we have demonstrated here a simple and straightforward strategy for the synthesis of IRMOF derived porous carbon materials with tunable porosity by varying the content of external carbonizing agent sucrose. We have used amine functionalized IRMOF-3 for efficient sucrose loading that acts as a template and also a self-sacrificing carbon precursor. Among various NPC samples, NPC-300 shows remarkable surface area with high micropore volume and good hydrogen and carbon dioxide storage properties. We have also demonstrated NPC-300 as electrode material for electrochemical double layer capacitor (EDLC). Our results would open up an avenue to synthesize versatile nanoporous carbon materials with tunable textural parameters derived from different porous MOFs with potential applications in gas storage and electrochemical supercapacitor.

Acknowledgments

The financial support (TKM) from DST (Govt. of India) and Sheikh Saqr fellowship is gratefully acknowledged. Authors are thankful to Prof. G.U. Kulkarni and Prof. C. Narayana for FESEM and Raman facilities respectively. Authors acknowledged Selvi (FESEM) and Usha (TEM) for microscopic measurements.

Appendix A. Supplementary data

Supplementary data associated with this article can be found, in the online version, at http://dx.doi.org/10.1016/j.micromeso.2014.12.008.

References

[1] F. Zhang, Y. Yu, Adv. Mater. Res. 621 (27–30) (2013) 25.
[2] W. Shen, W. Fan, J. Mater. Chem. A 1 (2013) 999–1013.
[3] H. Jiang, P.S. Lee, C. Li, Energy Environ. Sci. 6 (2013) 41–53.
[4] J.L. Figueiredo, J. Mater. Chem. A 1 (2013) 9351–9364.
[5] S.L. Candelaria, Y. Shao, W. Zhou, X. Li, J. Xiao, J.-G. Zhang, Y. Wang, J. Liu, J. Li, G. Cao, Nano Energy 1 (2012) 195–220.
[6] S.L. Candelaria, R. Chen, Y.-H. Jeong, G. Cao, Energy Environ. Sci. 5 (2012) 5619–5637.
[7] Y. Yang, K. Chiang, N. Burke, Catal. Today 178 (2011) 197–205.
[8] C. Liang, Z. Li, S. Dai, Angew. Chem. Int. Ed. 47 (2008) 3696–3717.
[9] C. Moreno-Castilla, F.J. Maldonado-Hodar, Carbon 43 (2005) 455–465.
[10] J.M. Calo, P.J. Hall, Carbon 42 (2004) 1299–1304.
[11] B. Nagel, S. Pusz, B. Trzebicka, J. Mater. Sci. 49 (2014) 1–17.
[12] D.D. Do, E.A. Ustinov, H.D. Do, Elsevier Ltd., 2008, pp. 239–271.
[13] G.-J. Lee, S.-I. Pyun, Mod. Aspects Electrochem. 41 (2007) 139–195.
[14] J.C. Dore, J.B.W. Webber, J.H. Strange, Colloids Surf. A 241 (2004) 191–200.
[15] F. Zhang, Y. Yu, Adv. Mater. Res. 621 (2013) 27–30.
[16] D.P. Upare, S. Yoon, C.W. Lee, Korean J. Chem. Eng. 28 (2011) 731–743.
[17] J. Lee, J. Kim, T. Hyeon, Adv. Mater. 18 (2006) 2073–2094.
[18] B. Sakintuna, Y. Yueruem, Ind. Eng. Chem. Res. 44 (2005) 2893–2902.
[19] M. Antonietti, N. Fechler, T.-P. Fellinger, Chem. Mater. 26 (2014) 196–210.
[20] M. Wang, Z.-H. Huang, Y. Bai, F. Kang, M. Inagaki, Curr. Org. Chem. 17 (2013) 1434–1447.
[21] J.L. Adcock, P.F. Fulvio, S. Dai, J. Mater. Chem. A 1 (2013) 9327–9331.
[22] N. Popovska-Leipertz, Elsevier Ltd., 2012, pp. 269–294.
[23] J. Gorka, R.T. Mayes, L. Baggetto, G.M. Veithb, S. Dai, J. Mater. Chem A 1 (2013) 3016–3026.
[24] L. Chuenchom, R. Kraehnert, B.M. Smarsly, Soft Matter 8 (2012) 10801–10812.
[25] Y. Xia, Z. Yang, R. Mokaya, John Wiley & Sons Ltd., 2011, pp. 217-264.
[26] S. Kubo, R. Demir-Cakan, L. Zhao, R.J. White, M.-M. Titirici, ChemSusChem 3 (2010) 188–194.
[27] J. Gorka, S. Dai, Elsevier Ltd., 2012, pp. 323–350.
[28] K.K.R. Datta, D. Jagadeesan, C. Kulkarni, A. Kamath, R. Datta, M. Eswaramoorthy, Angew. Chem. Int. Ed. 123 (2011) 4015–4019.
[29] L. Chuenchom, R. Kraehnert, B.M. Smarsly, Soft Matter 8 (2012) 10801–10812.
[30] L. Pan, K.-H. Li, J.Y. Lee, D.H. Olson, J. Li, John Wiley & Sons, Inc., 2009, pp. 307–352.
[31] Y. Yan, S. Yang, A.J. Blake, M. Schroder, Acc. Chem. Res. 47 (2014) 296–307.
[32] M. Sindoro, N. Yanai, A.-Y. Jee, S. Granick, Acc. Chem. Res. 47 (2014) 459–469.
[33] M. Li, D. Li, M. O'Keeffe, O.M. Yaghi, Chem. Rev. 114 (2014) 1343–1370.
[34] Z.R. Herm, E.D. Bloch, J.R. Long, Chem. Mater. 26 (2014) 323–338.
[35] M.L. Foo, R. Matsuda, S. Kitagawa, Chem. Mater. 26 (2014) 310–322.
[36] M. Yoon, K. Suh, S. Natarajan, K. Kim, Angew. Chem. Int. Ed. 52 (2013) 2688–2700.
[37] Y.-R. Lee, J. Kim, W.-S. Ahn, Korean J. Chem. Eng. 30 (2013) 1667–1680.
[38] N.A. Khan, Z. Hasan, S.H. Jhung, Adv. Porous Mater. 1 (2013) 91–102.
[39] H. Furukawa, K.E. Cordova, M. O'Keeffe, O.M. Yaghi, Science 341 (2013) 974.
[40] A. Dhakshinamoorthy, M. Opanasenko, J. Cejka, H. Garcia, Catal. Sci. Technol. 3 (2013) 2509–2540.
[41] G. Kumari, K. Jayaramulu, T.K. Maji, C. Narayana, J. Phys. Chem. A 117 (2013) 11006–11012.
[42] R. Kumar, K. Jayaramulu, T.K. Maji, C.N.R. Rao, Chem. Commun. 49 (2013) 4947–4949.
[43] K. Jayaramulu, N. Kumar, A. Hazra, T.K. Maji, C.N.R. Rao, Chem. Eur. J. 19 (2013) 6966–6970.
[44] K. Jayaramulu, R. Haldar, T.K. Maji, Polyhedron 52 (2013) 553–559.
[45] P. Kanoo, R. Matsuda, R. Kitaura, S. Kitagawa, T.K. Maji, Inorg. Chem. 51 (2012) 9141–9143.
[46] K. Jayaramulu, S.K. Reddy, A. Hazra, S. Balasubramanian, T.K. Maji, Inorg. Chem. 51 (2012) 7103–7111.
[47] P. Kanoo, G. Mostafa, R. Matsuda, S. Kitagawa, T.K. Maji, Chem. Commun. 47 (2011) 8106–8108.
[48] K. Jayaramulu, P. Kanoo, S.J. George, T.K. Maji, Chem. Commun. 46 (2010) 7906–7908.
[49] T.K. Maji, S. Kitagawa, Pure Appl. Chem. 79 (2007) 2155–2177.
[50] T.K. Maji, G. Mostafa, R. Matsuda, S. Kitagawa, J. Am. Chem. Soc. 127 (2005) 17152–17153.
[51] S. Pandiaraj, H.B. Aiyappa, R. Banerjee, S. Kurungot, Chem. Commun. 50 (2014) 3363–3366.
[52] H.B. Wu, S. Wei, L. Zhang, R. Xu, H.H. Hng, X.W. Lou, Chem. Eur. J. 19 (2013) 10804–10808.
[53] W. Chaikittisilp, K. Ariga, Y. Yamauchi, J. Mater. Chem. A 1 (2013) 14–19.

[54] S.J. Yang, T. Kim, J.H. Im, Y.S. Kim, K. Lee, H. Jung, C.R. Park, Chem. Mater. 24 (2012) 464–470.
[55] N. Reimer, B. Gil, B. Marszalek, N. Stock, CrystEngComm 14 (2012) 4119–4125.
[56] A. Banerjee, R. Gokhale, S. Bhatnagar, J. Jog, M. Bhardwaj, B. Lefez, B. Hannoyer, S. Ogale, J. Mater. Chem. 22 (2012) 19694–19699.
[57] M. Eddaoudi, J. Kim, N. Rosi, D. Vodak, J. Wachter, M. O'Keeffe, O.M. Yaghi, Science 295 (2002) 469–472.
[58] X. Cai, M. Peng, X. Yu, Y. Fu, D. Zou, J. Mater. Chem. C 2 (2014) 1184–1200.
[59] T. Tabikh, X. Huang, J. Energy Power Eng. 7 (2013) 1616–1623.
[60] M.E. Plonska-Brzezinska, L. EchegoyenJ, Mater. Chem. A 1 (2013) 13703–13714.
[61] M. Meyyappan, J. Vac. Sci. Technol., A 31 (2013). pp. 050803/050801–050803/050814.
[62] G. Feng, S. Li, V. Presser, P.T. Cummings, J. Phys. Chem. Lett. 4 (2013) 3367–3376.
[63] L. Dong, Z. Chen, D. Yang, H. Lu, RSC Adv. 3 (2013) 21183–21191.
[64] S. Kondrat, P. Wu, R. Qiao, A.A. Kornyshev, Nat. Mater. 13 (2014) 387–393.